J Appl Physiol 96: 1701–1713, 2004.
First published January 16, 2004; 10.1152/japplphysiol.01129.2003.

Role of heat shock protein 27 in cytoskeletal remodeling of the airway smooth muscle cell

Steven S. An,[1] Ben Fabry,[1] Mathew Mellema,[1] Predrag Bursac,[1] William T. Gerthoffer,[2] Usamah S. Kayyali,[3] Matthias Gaestel,[4] Stephanie A. Shore,[1] and Jeffrey J. Fredberg[1]

[1]*Physiology Program, Department of Environmental Health, Harvard School of Public Health, Boston, Massachusetts 02115;* [2]*Department of Pharmacology, University of Nevada, Reno, Nevada 89557;* [3]*Pulmonary and Critical Care Division, Tufts-New England Medical Center, Boston, Massachusetts 02111; and* [4]*Institute of Biochemistry, Hannover Medical School, 30625 Hannover, Germany*

Submitted 17 October 2003; accepted in final form 7 January 2004

An, Steven S., Ben Fabry, Mathew Mellema, Predrag Bursac, William T. Gerthoffer, Usamah S. Kayyali, Matthias Gaestel, Stephanie A. Shore, and Jeffrey J. Fredberg. Role of heat shock protein 27 in cytoskeletal remodeling of the airway smooth muscle cell. *J Appl Physiol* 96: 1701–1713, 2004. First published January 16, 2004; 10.1152/japplphysiol.01129.2003.—Remodeling of the airway smooth muscle (ASM) cell has been proposed to play an important role in airway hyperresponsiveness. Using a functional assay, we have assessed remodeling of the cultured rat ASM cell and the role of heat shock protein (HSP) 27 in that process. To probe remodeling dynamics, we measured spontaneous motions of an individual Arg-Gly-Asp-coated microbead that was anchored to the cytoskeleton. We reasoned that the bead could not move unless the microstructure to which it is attached rearranged; if so, then its mean square displacement (MSD) would report ongoing internal reorganizations over time. Each bead displayed a random, superdiffusive motion; MSD increased with time as $\sim t^{1.7}$, whereas an exponent of unity would be expected for a simple passive diffusion. Increasing concentrations of cytochalasin-D or latrunculin-A caused marked increases in the MSD, whereas colchicine did not. Treatments with PDGF or IL-1β, but not transforming growth factor-β, caused decreases in the MSD, the extent of which rank-ordered with the relative potency of these agents in eliciting the phosphorylation of HSP27. The chemical stressors anisomycin and arsenite each increased the levels of HSP27 phosphorylation and, at the same time, decreased bead motions. In particular, arsenite prevented and even reversed the effects of cytochalasin-D on bead motions. Finally, ASM cells overexpressing phospho-mimicking human HSP27, but not wild-type or phosphorylation-deficient HSP27, exhibited decreases in bead motions that were comparable to the arsenite response. Taken together, these results show that phosphorylated HSP27 favors reduced bead motions that are probably due to stabilization of the actin cytoskeleton.

cytoskeleton; plasticity; actin dynamics; diffusion; superdiffusion

AIRWAY HYPERRESPONSIVENESS (AHR) is a cardinal feature of asthma, but its mechanisms remain largely unexplained (37, 81). Evidence suggests that AHR may be attributable in part to alterations in the contractile behavior of the airway smooth muscle (ASM) cell (7, 70). In the ASM cell, myosin exerts its mechanical effects by interacting with actin within an integrated cytoskeletal (CSK) scaffolding (23, 61). It is now known that this scaffolding is dynamic and in a continuous state of remodeling; the actin lattice, the myosin filament, and the focal adhesion plaque of the ASM cell are all considered to be evanescent structures that can be virtually demolished in some circumstances and then reconfigured and stabilized in others (1, 4, 13, 22, 40, 53, 70, 71). The ability of the ASM cell to reorganize internal CSK structures to sustain tension generation over a wide range of working muscle lengths is thought to play an important role in AHR (24, 40, 61, 78, 79). However, underlying mechanisms and key molecules regulating CSK remodeling of the ASM cell remain quite unclear.

The 27-kDa heat shock protein (HSP27) is a member of the stress-inducible small heat shock protein family that is thought to act as a microfilament-capping protein in vitro (5, 55, 56). During cellular stress and growth, HSP27 is a target of post-translational modification and undergoes rapid phosphorylation (42, 44). Structural studies suggest that phosphorylation of HSP27 promotes actin polymerization and stress fiber formation (5, 21, 30, 47, 48, 59). In smooth muscle, HSP27 is constitutively expressed at high levels (6, 34, 55), and its phosphorylation causes colocalization of HSP27 with contractile proteins (32). In the ASM cell, Hedges and colleagues (26) have demonstrated that phosphorylation of HSP27 is a necessary condition for cell migration. Cell migration is an important mechanical event and must necessarily reflect some degree of CSK remodeling, but migration reflects many other processes as well (45, 57).

The present study was undertaken to focus specifically on functional remodeling of the cultured rat ASM cell and the role of HSP27 in that process. To probe the dynamics of CSK remodeling, we measured spontaneous movements of an individual microbead that was coated with a peptide containing the sequence Arg-Gly-Asp (RGD); such beads form focal adhesions and become anchored to the CSK via integrin receptors (51, 77). We reasoned that the bead cannot move unless the microstructure to which it is attached rearranges; if so, then bead motion, as quantified by its mean square displacement (MSD), would report the rate of ongoing internal rearrangements over time. To assess the contribution of HSP27 to these remodeling processes, we used growth factors, proinflammatory cytokines, and chemical stressors that are reported to phosphorylate HSP27 (21, 26). To assess the role of HSP27 more specifically, we transfected rat ASM cells so that they overexpressed either wild-type (HSP27-wt), phosphorylation-deficient (HSP27-uP), or phospho-mimicking human HSP27 (HSP27-P).

Address for reprint requests and other correspondence: S. S. An, Harvard School of Public Health, 665 Huntington Ave., Bldg. I, Rm. 1308, Boston, MA 02115 (E-mail: san@hsph.harvard.edu).

The costs of publication of this article were defrayed in part by the payment of page charges. The article must therefore be hereby marked "*advertisement*" in accordance with 18 U.S.C. Section 1734 solely to indicate this fact.

Others have inferred that HSP27 stabilizes the actin CSK based largely on structural evidence, especially the formation of filamentous (F)-actin measured by using fluorescent microscopy or other assays (21, 47, 48). Here we present a novel assay to measure the dynamics of underlying CSK remodeling, at the level of individual cells in culture, and provide direct functional evidence that phosphorylation of HSP27 indeed stabilizes the actin CSK, thus confirming inferences of others that were based solely on structural findings.

METHODS

Materials. Tissue culture reagents were obtained from Sigma (St. Louis, MO), with the exception of DMEM-Ham's F-12 (1:1), which was purchased from GIBCO (Grand Island, NY). The synthetic RGD peptide (Peptite 2000; Integra Life Sciences) was provided by Dr. Juerg Tschopp, and acetylated low-density lipoprotein (acLDL) was purchased from Molecular Probes (Eugene, OR). All drugs were obtained from Sigma. PDGF-AB, transforming growth factor-β (TGF-β), and IL-1β were reconstituted in sterile PBS. Cytochalasin-D, latrunculin-A, colchicines, and anisomycin were prepared in sterile DMSO. Arsenite was prepared in sterile distilled water. On the day of experiments, all reagents were diluted to final concentrations in serum-free media, yielding <0.1% PBS or 0.1% DMSO in final volume.

Animals. The Sprague-Dawley rats (female, 10–12 wk old) were obtained from a commercial supplier (Harlan, Indianapolis, IN) and housed in a conventional animal care facility at Harvard School of Public Health (Boston, MA). The protocols were approved by an Animal Ethics Committee.

Cell isolation and culture. Rat ASM cells were prepared as previously described (1). Rats were intraperitoneally injected with pentobarbital sodium (35 mg/kg), and the tracheas were aseptically excised and placed in Ca^{2+}, Mg^{2+}-free HBSS of the following composition (in mM): 5 KCl, 0.3 KH_2PO_4, 138 NaCl, 4 $NaHCO_3$, 0.3 Na_2HPO_4, and 1.0 glucose. The isolated tracheas were cleaned of connective tissues, cut longitudinally through the cartilage, and enzymatically dissociated with HBSS containing 0.05% elastase type IV and 0.2% collagenase type IV for 30 min in a shaking water bath at 37°C. Dissociated cells in suspension were centrifuged and resuspended in DMEM-Ham's F-12 medium (1:1) supplemented with 10% FBS and the antibiotics (100 U/ml penicillin, 100 μg/ml streptomycin, and 2.5 μg/ml amphotericin-β). Cells were plated on culture flasks and grew until confluence at 37°C in humidified air containing 5% CO_2. The media were changed every 3–4 days, and confluent cells were passaged with 0.25% trypsin-0.02% EDTA solution every 10–14 days. ASM cells in culture were elongated and spindle shaped, grew with the typical hill-and-valley appearance, and showed positive staining for the smooth muscle-specific proteins α-actin and calponin.

In the present study, we used cells in *passages 3–8*. To maximize the expression of smooth muscle-specific proteins and restore contractile phenotype, ASM cells at confluence were serum deprived and supplemented with 10 μg/ml insulin, 5.5 μg/ml transferrin, and 6.7 μg/ml sodium selenite for 24 h before cell seeding (1, 25, 50, 80). Unless otherwise specified, serum-deprived cells were plated at 30,000 cells/cm^2 on tissue culture petri dishes (9.6 cm^2 growth area; Becton Dickinson) previously coated with type I collagen (Vitrogen 100; Cohesion, Palo Alto, CA) at a concentration of 5 μg/ml. Cells were maintained in serum-free media for 24 h at 37°C in humidified air containing 5% CO_2. These conditions have been optimized for seeding cultured cells on collagen matrix and for assessing their mechanical properties (1, 29).

Characterization of spontaneous bead motion. To probe the dynamics of CSK remodeling, we measured spontaneous movements of an individual microbead that was coated with a peptide containing the sequence RGD; such beads bind avidly to cell surface integrin receptors, form focal adhesions, (51, 77), become well-integrated into the CSK scaffolding (1, 77), and display tight functional coupling to that scaffolding (13, 14, 51). As a control, we used beads that were coated with acLDL, which are linked to scavenger receptors thought to be floating in the cell membrane and thus not linked to focal adhesions (77).

Serum-deprived cells adherent on collagen-coated wells were incubated for 20 min with ~5×10^5 ferrimagnetic microbeads (4.5 μm in diameter) coated with synthetic RGD-containing peptides (50 μg peptide/mg beads) or acLDL (100 μg/mg beads) in serum-free media containing 1% BSA. Unbound beads were removed by washing cells with serum-free media. Under microscopic observation, we then visualized spontaneous displacements of individual microbeads (~100 beads per field of view) and recorded their positions every 83 ms as previously described (14). The trajectories of bead motions in two dimensions were characterized by computing the MSDs of all beads as function of time t, [MSD(t)] (nm^2)

$$\mathrm{MSD}(t) = \frac{1}{N}\sum_{i=1}^{N} r_i(t)^2 \qquad (1)$$

where $r_i(t)$ is the distance of the ith bead at time t relative to its position at $t = 0$. The MSDs were computed at intervals that were equally spaced in time (1.3 s). Bead motions were corrected for the confounding effects of microscope stage drift; the stage drift was estimated from changes of the mean position of all beads within a field of view. The limit of resolution in our system was on the order of ~10 nm, but by 10 s most beads had displaced a much greater distance. Accordingly, we analyzed MSD data for times >10 s and up to 300 s. As shown in RESULTS, the MSDs of microbeads increased with time according to a power law relationship

$$\mathrm{MSD}(t) = \mathrm{D}^* (t/t_o)^{\alpha} \qquad (2)$$

The coefficient D* and the exponent α of the bead motion were estimated from a least squares fit of a power law to the ensemble average of MSD data vs. time; we take t_o to be 1 s and express D* in units of nanometers squared. Separately, we computed, for each individual bead, the coefficient D* and the exponent α and compared and verified the estimates of these parameters using the former analysis. For ordinary Brownian motion, the distribution of displacements would be expected to be Gaussian and the exponent α to be unity, in which case the coefficient D* is the familiar diffusion coefficient in two dimensions (2, 38, 62, 66). When a power law relationship is shown to exist but the exponent α differs from unity, the random motions are said to reflect fractional diffusion (15); when the exponent α is smaller than unity, random motions are said to be subdiffusive; and when the exponent is larger than unity, random motions are said to be superdiffusive (15).

Over the course of 5 min, individual bead motions, as quantified by MSD(t), were evaluated both before and after each drug treatment. To modulate events leading to the formation of F-actin, ASM cells were treated for 10 min with increasing concentrations of direct actin-disrupting agents cytochalasin-D or latrunculin-A. Cytochalasin-D caps existing actin filaments at the barbed ends, whereas latrunculin-A prevents the assembly of actin monomers into F-actin (9, 10). To elicit HSP27 phosphorylation, ASM cells were treated for 20 min with growth factors (10 ng/ml PDGF or 1 ng/ml TGF-β) and the proinflammatory cytokine (6 ng/ml IL-1β) or for 1 h with chemical stressors (10 μM anisomycin or 200 μM sodium arsenite). Although these agents are known to activate multiple signaling pathways that could alter F-actin formation (11, 21, 27, 49, 60), the above conditions have been reported to cause optimal phosphorylation of HSP27 (21, 26).

Western blot analysis. The small mammalian heat shock proteins of the mouse (HSP25), Chinese hamster, and humans (HSP27) show similar structure and sequence in their genes (8, 16, 19, 28), share

>80% sequence homology in their amino acids (18, 46), and are reported to exhibit various common properties (5, 20, 21, 30, 33, 47, 48, 54). Studies have often used HSP27 interchangeably with HSP25 or variously called them still HSP25 (murine) or HSP27 (human). In this paper, we used "HSP27" to refer to both human and the endogenous rat HSP27 homolog, HSP25. As regards human HSP27 and murine HSP25, they differ in the number of their phosphorylation isoforms but have very similar major phosphorylatable serine residues Ser-82 (human) and Ser-86 (murine), located in the conserved kinase recognition sequence Arg-X-X-Ser (17, 43, 63). Therefore, we used phospho-HSP27 antibody specific for these serine residues (Cell Signaling, Woburn, MA) and measured changes in protein phosphorylation of HSP27 by Western blotting, as described below.

Confluent rat ASM cells in six-well plates were serum deprived for 24 h and treated with or without 10 ng/ml PDGF, 1 ng/ml TGF-β, 6 ng/ml IL-1β, 10 μM anisomycin, or 200 μM arsenite. Unless otherwise specified, ASM cells were treated for 0, 5, or 20 min with growth factors (PDGF and TGF-β) and the proinflammatory cytokine (IL-1β) and treated for 0, 30, or 60 min with chemical stressors (anisomycin and arsenite). After the indicated time, medium was withdrawn, and cells were washed twice with ice-cold PBS (10 mM Na_2HPO_4, 1.8 mM KH_2PO_4, 2.6 mM KCl, and 137 mM NaCl, pH 7.4) and lysed with 200 μl of extraction buffer (10 mM Tris·HCl buffer with 50 mM NaCl, 50 mM NaF, 10 mM D-serine, 1 mM EDTA, 1 mM EGTA, 1% SDS, 1% Triton X-100, 0.2 mM phenylmethylsulfonyl fluoride, 5 μg/ml leupeptin, 1 μg/ml pepstatin, 10^{-2} U/ml aprotinin). ASM cells were scraped off plates and repeatedly passed through a 25⅝-gauge needle. Protein concentration of the supernatant was determined by the Bradford method by using Bio-Rad dye reagent (Bio-Rad, Richmond, CA). Supernatants of cell lysates were then mixed with loading buffer [0.062 M Tris·HCl (pH 6.8), 10% glycerol, 2% SDS, 5% β-mercaptoethanol, and 0.01% (wt/vol) bromphenol blue] to a volume of 30 μl and boiled for 5 min. Equal amounts of total cell protein (30 μg/lane) were resolved by SDS-PAGE (125 V, 2 h) on 12% Tris-glycine gel (Invitrogen, Carlsbad, CA) and transferred to nitrocellulose membrane (16 V, 1 h) in transfer buffer (Invitrogen). Membranes were treated with blocking solution (10 mM Tris-saline buffer containing 150 mM NaCl, 0.1% Tween 20, and 5% nonfat dry milk), incubated overnight at 4°C with primary rabbit phospho-HSP27 antibody (dilution of 1:1,000; Cell Signaling), incubated for 1 h at room temperature with secondary goat anti-rabbit IgG linked to horseradish peroxidase (dilution 1:1,000; Cell Signaling), and then visualized by light emission on film with enhanced chemiluminescent substrate (Cell Signaling). The band visualized at ~25 kDa was scanned with a UMAX Powerlook flat-bed scanner (Bio-Rad, Hercules, CA) and analyzed by scanning densitometry with Gel Pro Analyzer software (Media Cybernetics, Silver Spring, MD). To correct for the differences in protein loading, the blots were reprobed with an antibody directed against murine HSP27 homolog (StressGen, British Columbia, Canada); total endogenous protein expression of HSP27 did not change for the duration of drug treatments (data not shown). All Western blotting experiments were performed at least three times.

The increase in protein phosphorylation in response to each agonist was separately normalized to total HSP27 expression, to baseline HSP27 phosphorylation, and to the maximum HSP27 phosphorylation; these normalizations did not alter the representation of the data, however. The increase in HSP27 phosphorylation is, therefore, expressed relative to bands of control samples (baseline) that were not treated with growth factors, the proinflammatory cytokine, or chemical stressors.

Transfection of the ASM cell. Confluent rat ASM cells were serum deprived for 24 h and passaged at 20,000 cells/cm^2 on tissue culture petri dishes (9.6 cm^2 growth area) previously coated with collagen. Cells were then maintained in DMEM-Ham's F-12 medium (1:1) supplemented with 1% FBS for 24 h, at which time the cell population reached more or less ~80% confluence. Adherent ASM cells were cotransfected with a green fluorescent protein (GFP)-expressing vector (pEGFP-N1 vector; Clontech, Palo Alto, CA) and the human HSP27 constructs of interest using Effectene (Qiagen, Valencia, CA), according to the manufacturer's instructions. The HSP27-uP mutant differs from the HSP27-wt in that the three known phosphorylation sites (Ser-15, Ser-78, and Ser-82) were mutated to alanine (43), whereas the HSP27-P replaced these phosphorylatable serine residues with negatively charged aspartates (63). HSP27-uP, HSP27-wt, and HSP27-P were cloned into pcDNA3 (Invitrogen) (63). The expression of human HSP27 proteins in cultured rat ASM cells was assayed by Western blotting by using an antibody directed against human HSP27 (UpState, Charlottesville, VA). In parallel experiments, the efficiency of transfection was assessed by Coulter ELITE flow cytometer (Coulter, Miami, FL); we typically obtained >30% transfection efficiency (data not shown).

On the day of experiments, cells were maintained in serum-free media. For each well of adherent ASM cells, we measured individual bead motions of both transfected and untransfected cells as visualized by fluorescent microscopic detection of GFP-expressing cells (see Fig. 8).

Statistical analysis. Data, unless otherwise noted, are presented as means ± SE; *n* represents the number of experiments. Student's *t*-test was used for statistical comparison of two means ($P < 0.05$ was considered significant).

RESULTS

Spontaneous bead motions were superdiffusive. Under microscopic observation, the serum-deprived ASM cells adhered firmly to collagen-coated dishes; they exhibited flat morphology with multiple vertexes at the two opposing ends of the cell and displayed no characteristic polar (asymmetric) morphology that is commonly observed in actively migrating cells (39, 67, 68). In each unstimulated ASM cell, we measured spontaneous movements of an individual RGD-coated microbead (4.5 μm in diameter) that was anchored to the CSK via integrin receptors (Fig. 1*A*). The trajectory of each bead displayed random motions (Fig. 1*B*). Over the course of 5 min, these motions amounted to only a small fraction of the bead diameter (~0.5 μm), however, and an even smaller fraction of cell size. As such, beads did not move from cell to cell. From the point of view of these very small bead motions, therefore, for all practical purposes, the cell would seem to be of virtually infinite lateral extent. Accordingly, the expectation would be that, for the duration of these experiments, bead motions would not be constrained by distant cell boundaries. Consistent with this interpretation, MSDs were found to grow in an unbounded fashion with time (Fig. 1*C*) and, more specifically, varied with time as a power law (*Eq. 2*).

When the beads were coated with RGD, the exponent α was systematically larger than unity [$\alpha = 1.54 \pm 0.30$ (SD)], whereas an exponent of unity would be expected for a simple passive diffusion. By contrast, beads coated with acLDL, which are linked to scavenger receptors thought to be floating in the cell membrane, and thus not linked to focal adhesions, exhibited an exponent substantially smaller ($P < 0.05$) but still bigger than unity [$\alpha = 1.31 \pm 0.39$ (SD)]. Although the exponent α was smaller, the coefficient D* (245.6 ± 11.4) was more than an order of magnitude greater compared with RGD-coated beads (25.2 ± 1.2), suggesting that beads coated with acLDL were very mobile compared with beads that were coated with RGD. Moreover, RGD-coated beads of different diameters (over a 3-fold range, from 1.6 to 4.8 μm) showed no differences in the exponent α or the coefficient D* (P. Bursac,

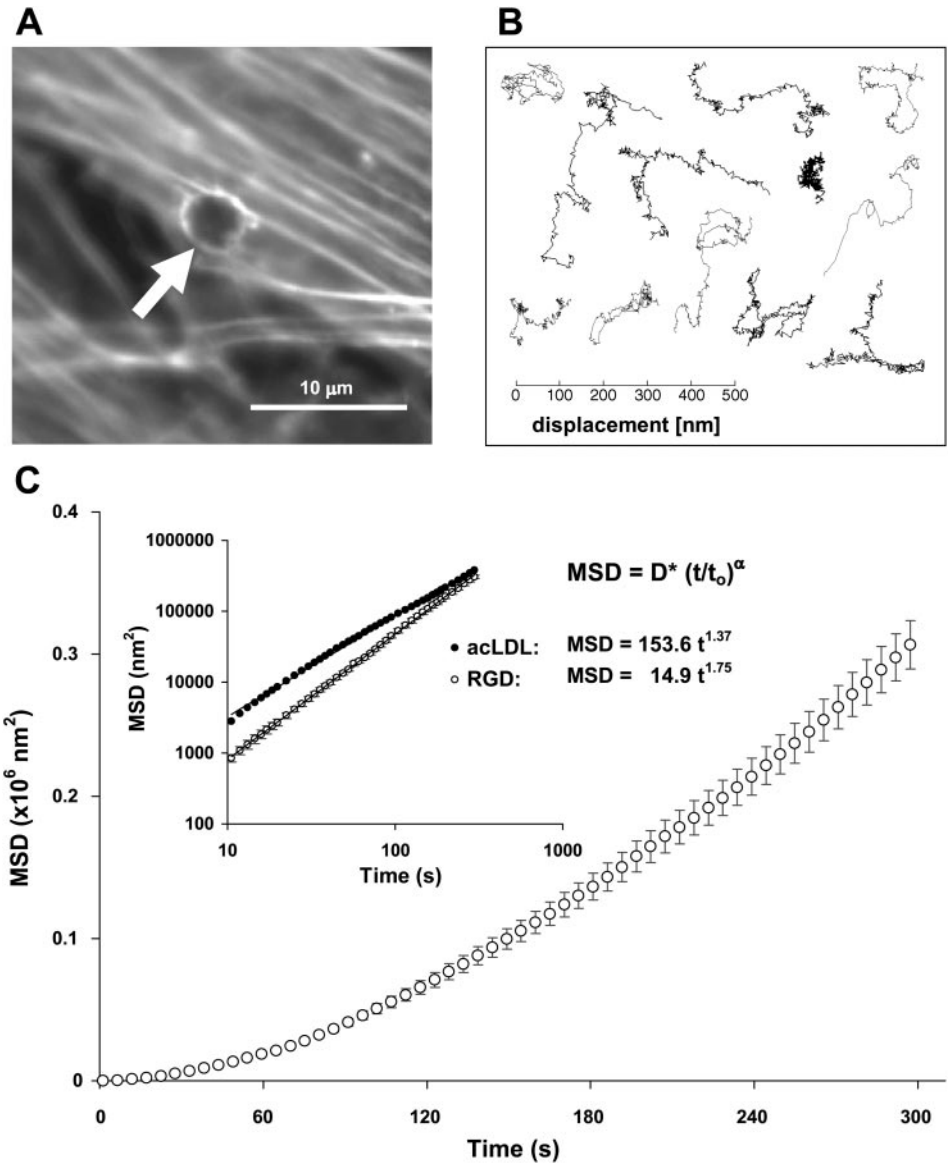

Fig. 1. Spontaneous bead motions report ongoing internal rearrangements. *A*: individual Arg-Gly-Asp (RGD)-coated microbead (arrow) binds avidly to the actin cytoskeleton (CSK) (stained with phalloidin) of the cultured airway smooth muscle (ASM) cell. *B*: under microscopic observation, each RGD-coated bead undergoes spontaneous random displacements (a representative tracing) as the CSK to which it is connected explores different internal configurations. *C*: spontaneous bead motions are quantified by their mean square displacements (MSD) as function of time (*Eq. 1*); the MSD increases with time according to a power law relationship. The coefficient D* and the exponent α of the bead motion were estimated from a least squares fit of a power law to the MSD data vs. time. *Inset*: the MSD of RGD-coated beads (○; 50 μg peptide/mg beads) increases with time (t) as $\sim t^{1.7}$ (the same data in logarithmic coordinates), whereas an exponent of unity would be expected for a simple passive diffusion. By contrast, spontaneous motions of beads coated with acetylated low-density lipoprotein (●; acLDL; 100 μg acLDL/mg beads) are quite mobile and exhibit substantially smaller exponent α. Here, and in all subsequent figures, the MSDs were computed at intervals that were equally spaced in time (1.3 s). For clarity, however, we have suppressed many of these data and left only data at approximately logarithmically spaced intervals. Values are means ± SE (n = 31–45 wells; 2,521–4,084 cells).

personal communication), whereas, in the case of simple Brownian motion, the coefficient D* would be expected to decrease by threefold. Finally, experiments conducted on micropatterned substrates, on which the cell could adhere but not crawl (58), showed the same superdiffusive behavior of RGD-coated beads (P. Bursac, personal communication). Taken together, these findings suggest that the superdiffusive behavior of RGD-coated beads was not driven by thermal forces, as in simple diffusion, or by cell crawling. These findings suggest instead that these motions reflect ongoing internal rearrangements of CSK structures to which beads were tethered.

Effects of cytochalasin-D and latrunculin-A on CSK stability. After a 10-min incubation with an actin-disrupting agent, cytochalasin-D (1–10 μM), bead motions as quantified by the MSD remained superdiffusive and, at the same time, showed an increase from baseline control (before drug treatments) of more than an order of magnitude (Fig. 2). The increase in bead motions was accounted for by a slight increase in the exponent α [from 1.47 ± 0.30 (SD) to 1.61 ± 0.31 at 1 and 10 μM, respectively] but mostly by a large increase in the coefficient D* (from 23.8 ± 1.3 to 51.7 ± 4.9 at 1 μM and to 107.7 ± 10.1 at 10 μM). In their effects on the net MSDs, 1 μM latrunculin-A and 10 μM cytochalasin-D were equally potent (Fig. 2). Colchicine (10 μM administered for 10 min), an agent that disrupts microtubule assembly, caused only a small increase in both the exponent α and the coefficient D*, and thus the MSD evaluated at 300 s was not statistically different compared with that of the baseline control (Fig. 2). ASM cells incubated for 10 min with or without 0.1% DMSO (the vehicle used for these agents) in serum-free media did not exhibit a significant change in bead motions compared with that of the baseline control (data not shown).

Effects of PDGF, TGF-β, and IL-1β on CSK stability. Hedges and colleagues (26) have demonstrated that the growth factors PDGF and TGF-β and the proinflammatory cytokine IL-1β promote canine ASM cell migration by activating the p38 mitogen-activated protein (MAP) kinase pathway leading to the phosphorylation of HSP27. In cultured rat ASM cells, we

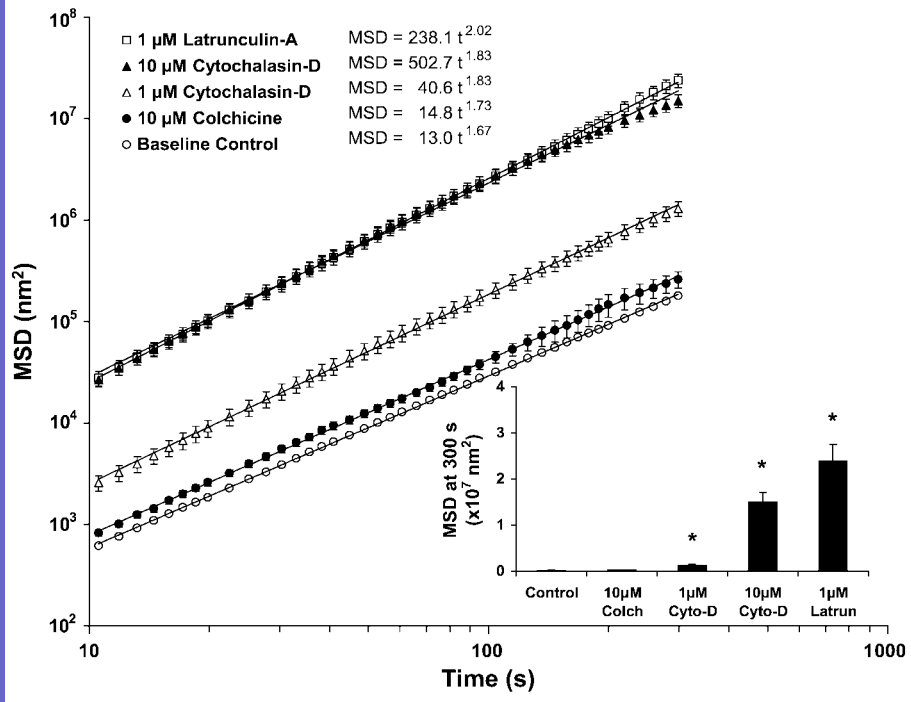

Fig. 2. Cytochalasin-D and latrunculin-A cause a marked increase in bead motions, whereas colchicine does not. ASM cells were treated for 10 min with or without cytochalasin-D (1 or 10 μM), latrunculin-A (1 μM), or colchicine (10 μM). Bead motions were measured both before and after each drug treatment; the coefficient D* and the exponent α of the bead motion were estimated from a least squares fit of a power law to the MSD data vs. time. ○, Baseline MSD before each drug treatment; baseline MSD from all cells were combined. ●, MSD after 10 μM colchicine treatment; △, after 1 μM cytochalasin-D; ▲, after 10 μM cytochalasin-D; □, after 1 μM latrunculin. *Inset:* MSD evaluated at 300 s of ASM cells treated with each drug. Values are means ± SE (n = 4–12 wells; 284–1,240 cells). *Significant difference from baseline MSD evaluated at 300 s (control), $P < 0.05$.

measured the level of HSP27 phosphorylation induced by PDGF, TGF-β, or IL-1β and evaluated the effects of these agents on spontaneous bead motions. PDGF (10 ng/ml) and IL-1β (6 ng/ml) each elicited a time-dependent phosphorylation of HSP27, whereas TGF-β (1 ng/ml) did not (Fig. 3). The peak phosphorylation was observed at 20 min.

ASM cells treated for 20 min with PDGF or IL-1β exhibited a decrease in bead motion, whereas cells treated with TGF-β did not show statistical changes in the net MSDs from that of untreated cells (Fig. 4). The extent of the decrease rank ordered with the relative potency of these agents in eliciting HSP27 phosphorylation (TGF-β < IL-1β < PDGF): the greater was the phosphorylation of HSP27, and the smaller were the bead motions. A time-matched treatment (20 min) with or without 0.1% PBS (the vehicle used for these agents) in serum-free media did not decrease the MSD (data not shown).

Effects of anisomycin and arsenite on CSK stability. To further assess the contribution of HSP27 phosphorylation to

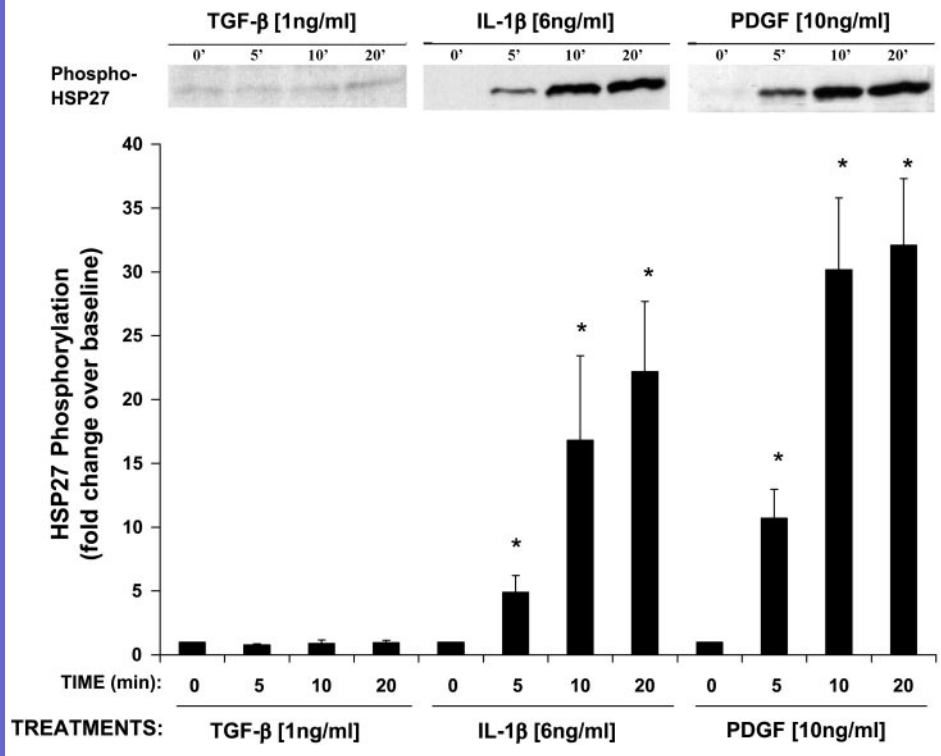

Fig. 3. PDGF, transforming growth factor-β (TGF-β), and IL-1β elicit varying degrees of 27-kDa heat shock protein (HSP27) phosphorylation. ASM cells were incubated for 0, 5, 10, and 20 min with TGF-β (1 ng/ml), IL-1β (6 ng/ml), or PDGF (10 ng/ml). After the indicated time, cells were lysed, and proteins were sequentially resolved by SDS-PAGE, transferred to nitrocellulose membrane, probed with rabbit antibody specific for the phosphorylated HSP27, and detected with secondary goat anti-rabbit IgG linked to horseradish peroxidase. The increase in protein phosphorylation is expressed as relative to the control sample (*time 0*) that was not treated with growth factors or cytokine. Values are means ± SE (n = 3 wells). *Significant difference from the control, $P < 0.05$.

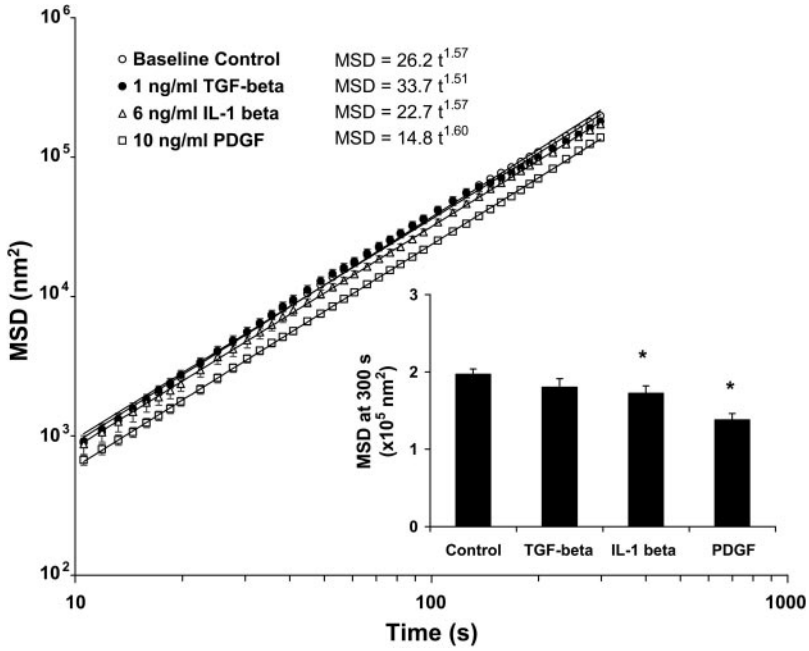

Fig. 4. PDGF, TGF-β, and IL-1β cause a slight decrease in bead motions. ASM cells were incubated for 20 min with or without TGF-β (1 ng/ml), IL-1β (6 ng/ml), or PDGF (10 ng/ml). Bead motions were measured both before and after each treatment; the coefficient D* and the exponent α of the bead motion were estimated from a least squares fit of a power law to the MSD data vs. time. ○, Baseline bead MSD before each treatment; baseline MSD from all cells were combined. ●, MSD after TGF-β treatment; △, after IL-1β; □, after PDGF. *Inset*: the MSD evaluated at 300 s of ASM cells treated with or without TGF-β, IL-1β, or PDGF. Values are means ± SE (n = 8–17 wells; 867–1,742 cells). *Significant difference from baseline MSD evaluated at 300 s (control), $P < 0.05$.

observed changes in bead motions, we used anisomycin and arsenite, both of which are known to activate MAP kinases, leading to the phosphorylation of HSP27 (21, 35, 49, 60, 65). ASM cells treated with anisomycin (10 μM) or arsenite (200 μM) exhibited time-dependent increases in the level of HSP27 phosphorylation, of which the peak phosphorylation (~20-fold increase from baseline) was observed at 1 h (Fig. 5).

After a 1-h incubation with anisomycin or arsenite, bead motions decreased substantially from baseline control; changes of both the exponent α and the coefficient D* contributed importantly to these changes (Fig. 6). ASM cells treated with anisomycin or arsenite exhibited an ~44 or 57% reduction of the MSD evaluated at 300 s, respectively, from baseline control (Fig. 6). A time-matched treatment (1 h) with serum-free media did not decrease the MSD, however (data not shown).

Based largely on structural evidence, others have inferred that phosphorylation of HSP27 stabilizes the actin CSK and confers resistance against not only the effects of heat shock and

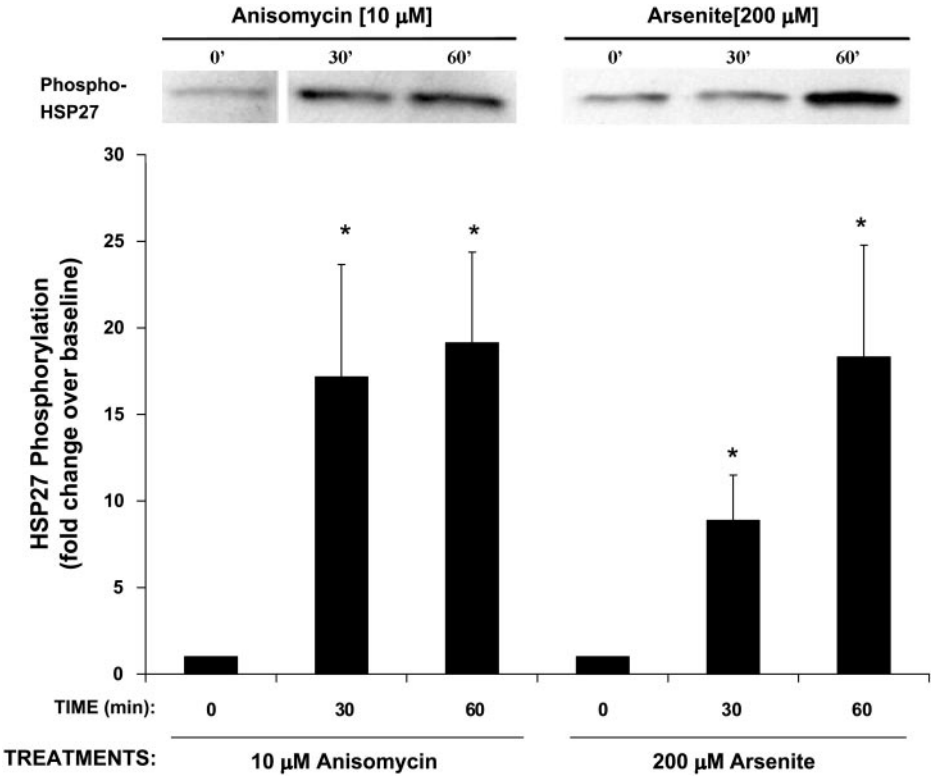

Fig. 5. Anisomycin and arsenite elicit the phosphorylation of HSP27. ASM cells were incubated for 0, 30, and 60 min with anisomycin (10 μM) or arsenite (200 μM). After the indicated time, cells were lysed, and proteins were sequentially resolved by SDS-PAGE, transferred to nitrocellulose membrane, probed with rabbit antibody specific for the phosphorylated HSP27, and detected with secondary goat anti-rabbit IgG linked to horseradish peroxidase. The increase in protein phosphorylation is expressed as relative to the control sample (*time 0*) that was not treated with chemical stressors. Values are means ± SE (n = 5–12 wells). *Significant difference from the control, $P < 0.05$.

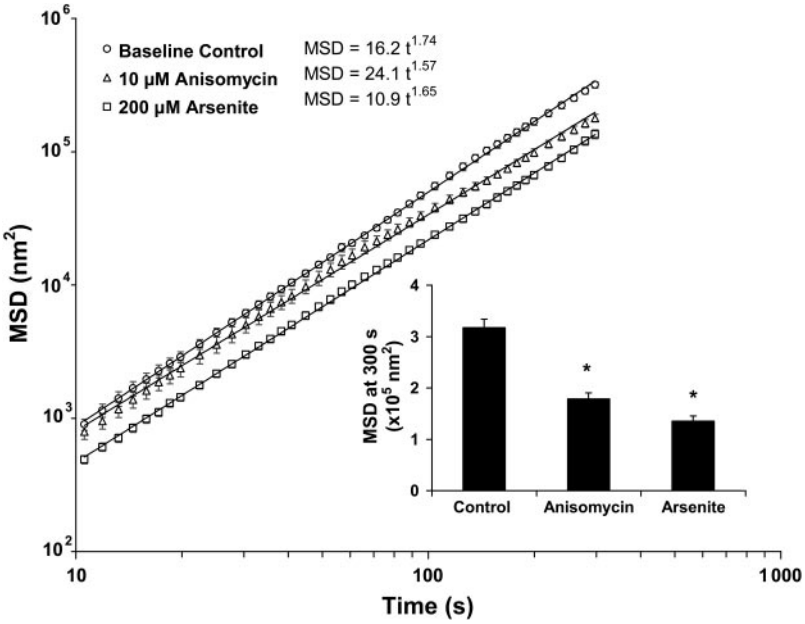

Fig. 6. Anisomycin and arsenite cause a marked decrease in bead motions. ASM cells were incubated for 60 min with or without anisomycin (10 μM) or arsenite (200 μM). Bead motions were measured both before and after each treatment; the coefficient D* and the exponent α of the bead motion were estimated from a least squares fit of a power law to the MSD data vs. time. ○, Baseline bead MSD before each drug treatment; baseline MSD from all cells were combined. △, MSD after anisomycin treatment; □, after arsenite. *Inset*: the MSD evaluated at 300 s of ASM cells treated with or without anisomycin or arsenite. Values are means ± SE (n = 17–18 wells; 1,034–1,350 cells). *Significant difference from baseline MSD evaluated at 300 s (control), $P < 0.05$.

oxidative stress, but also cytochalasin-D (21, 30, 47, 48). Thus we evaluated the relationship, if any, between the phosphorylated state of HSP27 and the ability of the ASM cell to maintain the stability of the actin CSK against the actin-disrupting agent cytochalasin-D. ASM cells were treated for 1 h with 200 μM arsenite to maximally phosphorylate HSP27. We measured the effects of arsenite on bead motions either before or after a 10-min treatment with 1 μM cytochalasin-D. ASM cells treated with arsenite exhibited a decrease in bead motions compared with the baseline control and, more interestingly, showed restricted bead motions even after a 10-min challenge with cytochalasin-D (Fig. 7; *protocol 1*). On the other hand, ASM cells treated first with a 10-min challenge with cytochalasin-D exhibited an increase in bead motions compared with the baseline control but showed a substantial decrease in bead motions after a 1-h treatment with 200 μM arsenite (Fig. 7; *protocol 2*). For control, ASM cells treated with a 10-min challenge with cytochalasin-D exhibited an increase in bead motions that remained elevated even after 1 h (Fig. 7; *protocol 3*). Taken together, these findings suggest that the phosphorylated state of HSP27 not only stabilizes the actin CSK but also prevents and even reverses the actions of actin-disrupting agent cytochalasin-D.

Effects of HSP27 overexpression on CSK stability. All of the agents used above lead to the phosphorylation of HSP27 but are known to activate multiple signaling pathways and are thereby nonspecific in that regard (11, 21, 27, 49, 60). To assess the specific contribution of HSP27 to spontaneous bead motions, ASM cells were transiently cotransfected with a GFP-expressing vector and the human HSP27 constructs of interest. The HSP27-uP differed from the HSP27-wt in that the three known phosphorylation sites (Ser-15, Ser-78, and Ser-82) were mutated to alanine (43), whereas the HSP27-P replaced these phosphorylatable serine residues with negatively charged aspartates (63). For control, ASM cells were transfected with the GFP-expressing vector only. For each well of adherent ASM cells, we measured individual bead motions of both transfected and untransfected cells as visualized by fluorescent microscopic detection of GFP-expressing cells (Fig. 8).

ASM cells overexpressing the HSP27-uP showed no statistical difference in bead motions compared with that of either untreated control or GFP-transfected cells (Fig. 8*C*). In contrast, overexpression of the HSP27-wt caused increases, whereas the HSP27-P caused decreases in bead motions (Fig.

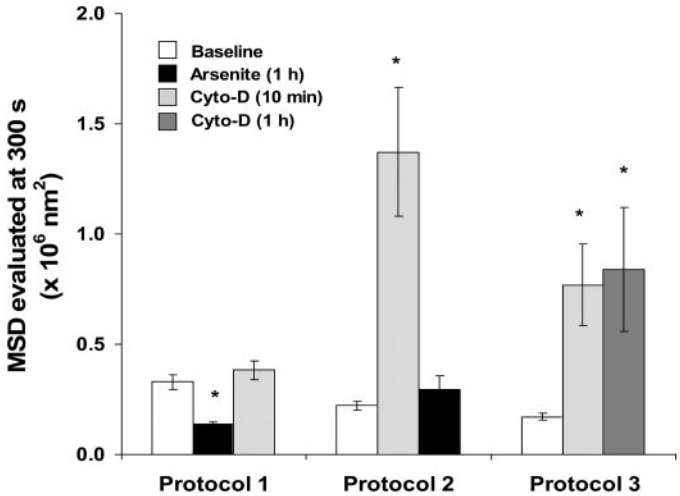

Fig. 7. Arsenite stabilizes the CSK. *Protocol 1*, ASM cells were first incubated for 1 h with arsenite (200 μM) and subsequently treated for 10 min with cytochalasin-D (1 μM). *Protocol 2*, ASM cells were first treated for 10 min with cytochalasin-D (1 μM) and subsequently treated for 1 h with arsenite (200 μM). *Protocol 3*, ASM cells were incubated up to 1 h with cytochalasin-D (1 μM). For each protocol, the MSD was measured both before and after each treatment; only the MSD evaluated at 300 s is shown. Open bars, initial baseline bead MSD at 300 s; solid bars, a 1-h arsenite treatment; light shaded bars, a 10-min cytochalasin-D treatment; dark shaded bars, a 1-h cytochalasin-D treatment. Values are means ± SE (n = 4–8 wells; 363–1,047 cells). *Significant difference from the baseline MSD evaluated at 300 s of each protocol, $P < 0.05$.

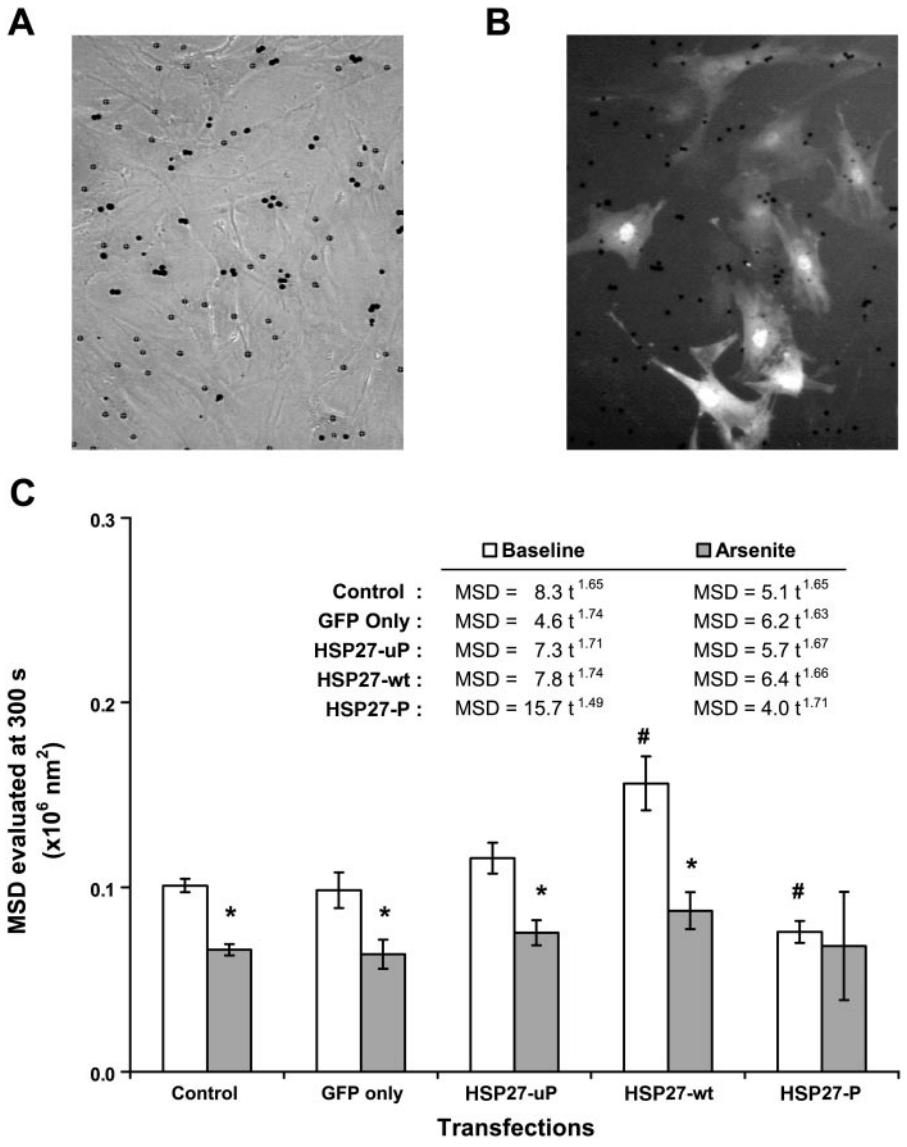

Fig. 8. Phosphorylated HSP27 tethers bead motions. ASM cells were transiently cotransfected with a green fluorescent protein (GFP)-expressing vector and the human HSP27 constructs of interest. For control, cells were transfected with the GFP-expressing vector only. *A*: bright-field image of ASM cells showing both transfected and untransfected cells. *B*: same field of view as visualized by fluorescent microscopic detection of GFP-expressing cells (transfected cells). *C*: bead MSD were measured both before and after arsenite treatment (1 h). Open bars, baseline bead MSD evaluated at 300 s of ASM cells transfected with or without GFP, wild-type human (HSP27-wt), phosphorylation-deficient (HSP27-uP), or phospho-mimicking (HSP27-P) HSP27 mutants. Shaded bars, the MSD evaluated at 300 s of cells treated for 1 h with 200 μM arsenite. Values are means ± SE (n = 3–23 wells; 27–388 cells). *Significant difference from baseline MSD evaluated at 300 s for each group, $P < 0.05$. #Significant difference from baseline MSD of untransfected cells (control), $P < 0.05$.

8*C*); these changes were statistically different from each of the other transfected or untransfected cells. Under baseline conditions, therefore, ASM cells overexpressing the HSP27-uP or the HSP27-wt exhibited substantial increases in bead motions compared with those overexpressing the HSP27-P.

After a 1-h incubation with 200 μM arsenite, each cell (untransfected control, GFP control, HSP27-wt, and HSP27-uP) exhibited significant decreases in bead motions that were comparable to the cell overexpressing the HSP27-P (Fig. 8*C*). The extent to which arsenite caused decreases in bead motions for the HSP27-uP (~35%) was similar to that of the controls (untransfected and GFP transfected) but was less than that of the HSP27-wt (~44%), however. ASM cells overexpressing the HSP27-P did not exhibit further decreases in bead motions in response to arsenite (Fig. 8*C*).

DISCUSSION

Spontaneous motions of an individual RGD-coated microbead that was anchored to the CSK were random, unbounded, and superdiffusive. Actin-disrupting agents cytochalasin-D or latrunculin-A caused marked increases in bead motions, whereas microtubule-disrupting agent colchicine did not. Growth factors, cytokines, or chemical stressors that lead to the phosphorylation of HSP27, in contrast, caused decreases in bead motions; the most potent among these, the chemical stressor arsenite, prevented and even reversed the effects of cytochalasin-D on bead motions. Overexpression of a HSP27-P mutant, but not HSP27-wt or HSP27-uP, caused decreases in bead motions that were comparable to the arsenite response. Taken together, these results suggest that phosphorylated HSP27 functionally stabilizes internal CSK structures.

Like the CSK of many cell types, that of the ASM cell is in a continuous state of remodeling. In particular, the ASM cell has the ability to adapt its optimal length over an impressively wide range, approaching threefold variations of optimal length in the same muscle within a time frame of ≤1 h (23, 24, 40, 61, 79). The ability of the ASM cell to reorganize internal CSK structures to sustain tension generation over a wide range of working muscle lengths may play an important role in AHR, but the mechanisms and molecules regulating CSK remodeling

of the ASM cell remain unclear. The findings reported here suggest a role for HSP27 in these remodeling processes.

Bead tethering and superdiffusive behavior. A bead coated with a peptide containing the sequence RGD binds avidly to integrins, forms focal adhesions (51, 77), becomes well-integrated into the CSK scaffolding (Fig. 1), and displays tight functional coupling to that scaffolding (14, 51). A bead coated with acLDL, by contrast, binds to scavenger receptors and shows none of these distinctive characteristics (77).

Spontaneous motions of beads coated with RGD vs. acLDL were qualitatively similar (i.e., both exhibited superdiffusive behavior) but quantitatively different. Compared with beads coated with RGD, those coated with acLDL were much more mobile at small times (i.e., the coefficient D* was larger by an order of magnitude), but the superdiffusive exponent (α) was substantially smaller (Fig. 1). At this time, we do not know to what extent beads coated with acLDL are integrated, if at all, to the underlying actin CSK, however. The former, by contrast, were far less mobile (by an order of magnitude or more) but increased their MSDs systematically faster than linearly with time, displaying a power law dependence on time with the exponent falling in the range of 1.6–1.8. Moreover, these superdiffusive random displacements were not sensitive to bead size. These observations for RGD-coated beads, taken together, are inconsistent with simple Brownian motion. Instead, they are consistent with the notion that these beads tracked motions of underlying structures to which they are attached and that those motions are superdiffusive.

We considered the possibility that the observed superdiffusive behavior of RGD-coated beads might be attributable to transfer of beads between integrin receptors or to cell migration. However, there are a number of arguments against these ideas. Under microscopic observation, the serum-deprived ASM cells adhered firmly to collagen-coated dishes; they exhibited flat morphology with multiple vertexes at the two opposing ends of the cell and displayed no characteristic polar (asymmetric) morphology that is commonly observed in actively migrating cells (39, 67, 68). In addition, the strong attachment of the beads to the cytoskeleton by RGD-integrin binding is well established (1, 14, 29, 51, 76, 77), and the development of focal adhesions and complex interconnections to the actin CSK matrix is readily observed at the bead locations (51, 77). Indeed, when the actin cytoskeleton was disrupted by cytochalasin-D or latrunculin-A, bead motions were greatly increased, perhaps by the direct disruption of the actin microfilament network but possibly through disconnection of the cytoskeleton from the integrin molecules attached to the beads. Finally, experiments conducted on micropatterned substrates on which the cell could adhere but not crawl (58) showed the same superdiffusive behavior of RGD-coated beads.

Simple diffusive motions arise when a particle is subjected to a time series of impulsive forces that are random and mutually independent. Resulting incremental motions are uncorrelated in time, and the MSD increases linearly in time. Superdiffusive motions, by contrast, imply correlation in the forcing time series and, in particular, persistence (15). That is to say, compared with the preceding incremental displacement, the next incremental displacement is likely to be in the same direction; resulting motions are still random with zero mean drift but are correlated over time and display a MSD that increases with an exponent greater than unity. Finally, subdiffusive motions imply correlation in the forcing as well, but one that leads to antipersistence; the MSD grows in time but with an exponent smaller than unity. Diffusive, superdiffusive, and subdiffusive behaviors fall under the unifying rubric of fractional Brownian motion and are often interpreted in terms of Levy walks (15).

Taken together, the findings reported here suggest that spontaneous motions of an individual RGD-coated microbead were not driven passively by thermal forces as in ordinary Brownian diffusion, receptor-coupling dynamics, or cell crawling, but rather were influenced by active, ongoing, and internal rearrangements of the CSK to which beads were tethered. These findings are consistent with the idea that the CSK is in a continuous state of remodeling; they also extend that idea and quantify it. These findings show that the rate of CSK remodeling appears to be a regulated variable and that the underlying mechanism, whatever it might be, displays features of a superdiffusive process.

Molecules and structures. What molecules and CSK structures might account for the active remodeling of the ASM cell? The CSK is a complex structure composed of scores of CSK and signaling molecules. It remains unclear, however, how these individual molecules are interconnected and, in particular, how each contributes to the remodeling of the ASM cell. Previously, our laboratory (1) and others (53) have shown that cytochalasin-D and latrunculin-A decrease the formation of F-actin and the force generation of smooth muscle. In the cultured human ASM cell, Stamenovic and colleagues (73) have demonstrated that 1 μM colchicine is sufficient to disrupt a substantial fraction of microtubules; the filamentous pattern of microtubules gradually disappears and becomes disorganized within 15 min of the treatment. The apparent structural changes caused by colchicine amounted to only a fractional change in the contractile stress, however (73). In nonmuscle cells, the disruption of actin microfilaments or microtubules not only lessens CSK integrity (76) but also impairs cell migration (72).

Here we have assessed the contribution of actin and microtubule dynamics to spontaneous bead motions. ASM cells treated with the actin-disrupting agents cytochalasin-D or latrunculin-A showed a marked increase in bead motions from baseline control (before drug treatments) of more than one order of magnitude (Fig. 2). ASM cells treated with colchicine at concentrations up to 10 μM, however, failed to exhibit appreciable changes in overall MSD from baseline control (Fig. 2). Although we cannot rule out the importance of microtubules in CSK integrity and cell migration, over the time scales probed by our measurements, the dynamics of microtubule assembly and disassembly did not seem to modulate bead motions.

Both cytochalasin-D and latrunculin-A caused an increase in bead motions that was accounted for by increases in both the coefficient D* and the exponent α (Fig. 2). These agents act via distinct modes of action to block the formation of F-actin: cytochalasin-D caps existing actin filaments at the barbed ends, whereas latrunculin-A prevents the assembly of monomeric (G) actin into F-actin (9, 10). It seems likely that the dramatic increase in bead motions caused by these agents reflects disruptions and/or changes in actin dynamics, resulting in net depolymerization of F-actin. As regards the disruption of

F-actin, the increase in the coefficient D* would be expected because the bead would be less tethered to the underlying actin CSK and thereby would move much more freely. Nevertheless, this is not sufficient to explain the increase in the exponent α. Although we do not understand the mechanism(s) and, in particular, what is driving the persistence of bead motions (15, 57, 75), the active remodeling of the ASM cell as measured by bead motions may be largely accounted for by the underlying dynamics of actin CSK.

HSP27 and CSK remodeling. In canine ASM cells, Hedges and colleagues (26) used a cell migration assay to examine actin CSK remodeling and its changes in response to numerous growth factors and proinflammatory cytokines. Although these agents are known to activate multiple signaling pathways that could alter F-actin formation (11, 21, 27), these authors demonstrated that cell migration requires phosphorylation of the HSP27. HSP27 is a member of the stress-inducible small heat shock protein family that is thought to act as a microfilament-capping protein in vitro (5, 55, 56). The amino acid sequence of human, mouse, and Chinese hamster HSP27s is highly conserved (16, 18, 19, 28, 46), and all contain a number of the putative protein kinase phosphorylation site motif Arg-X-X-Ser (17, 43). There are three phosphorylation sites on human HSP27 (denoted as Ser-15, Ser-78, and Ser-82), whereas there are only two such sites in rodents on Ser-15 and Ser-86 (corresponding to human Ser-82). In humans, two phosphorylated isoforms (Ser-78 and Ser-82) are observed with various stimulations (heat shock, phorbol ester, tumor necrosis factor, serum, thrombin, fibroblast growth factor, and sodium arsenite), and the third phosphorylated isoform (Ser-15) is observed with sodium arsenite (43). In rodents, arsenite as well as PKC and PKA stimuation cause a rapid phosphorylation of HSP27 on Ser-15 and Ser-86 (17). Collectively, it appears that the major phosphorylation site of HSP27 is on Ser-82 (human) and Ser-86 (rodent) (17, 43, 63). In the present study, we used phospho-HSP27 antibody specific for these serine residues and measured changes in protein phosphorylation of HSP27 by Western blotting; therefore, we cannot explain definitely the effects of various agonists (PDGF, IL-1β, and TGF-β) on the specific site of phosphorylation. In addition, we cannot explain the strict order in which they are phosphorylated or the functional consequences, if any, of each phosphorylated isoforms.

In cultured rat ASM cells, PDGF (10 ng/ml) and IL-1β (6 ng/ml) both elicited a time-dependent phosphorylation of HSP27, whereas TGF-β (1 ng/ml) elicited no detectable change (Fig. 3). In canine ASM cells, Hedges and colleagues (26) found generally similar results except in the case of TGF-β, where a 20-min stimulation with the same concentration of TGF-β caused a sixfold increase in the phosphorylation of HSP27. Although we do not know whether this difference is due to species specificity, concentration dependency, or the differences in the assays used, the levels of HSP27 phosphorylation induced by TGF-β in their study, as in ours, were consistently smaller compared with that induced by PDGF or IL-1β. Moreover, ASM cell migration in response to TGF-β was substantially less compared with that of PDGF or IL-1β (26). In human aortic vascular smooth muscle cells, a 10-fold higher concentration of TGF-β than what was used here does not stimulate their migration but instead attenuates cell migration elicited by PDGF (12). Similarly, we found that ASM cells treated for 20 min with PDGF or IL-1β, but not TGF-β, exhibited a decrease in bead motions (Fig. 4). In fact, the extent of the decrease rank ordered with the relative potency of these agents in eliciting the phosphorylation of HSP27: the more phosphorylated HSP27, the more bead motions decreased from baseline.

The signaling pathways regulating HSP27 phosphorylation are fairly well established; HSP27 lies downstream of the p38 MAP kinase cascade, in which p38 MAP kinase-mediated activation of MAP kinase-activated protein kinase-2/3 (MAPKAP kinase 2/3) leads to the phosphorylation of HSP27 (21, 44, 65). To further assess the contribution of HSP27 phosphorylation to the observed changes in bead motions, we used anisomycin and arsenite, both of which are known to activate MAP kinases, leading to the phosphorylation of HSP27 (21, 35, 49, 60, 65). ASM cells treated with anisomycin (10 μM) or arsenite (200 μM) exhibited time-dependent increases in the level of HSP27 phosphorylation, of which the peak phosphorylation was observed at 1 h (Fig. 5). Both anisomycin and arsenite caused substantial decreases in bead motions (Fig. 6). Interestingly, however, the extent to which chemical stressors (anisomycin and arsenite) and growth factors (IL-1β and PDGF) caused decreases in bead motions was different (Figs. 4 and 6). These differences could not be solely accounted for by their rank-ordered potency of eliciting HSP27 phosphorylation. At this time, we cannot explain these differences, because these agonists are known to activate multiple signaling pathways (21, 26, 27, 35, 49, 60, 65) and their modes of action could be much more complex. What is clear, nevertheless, is that signals that lead to the phosphorylation of HSP27 decreased bead motions.

HSP27 and CSK stability. Based largely on structural evidence, others have inferred that phosphorylation of HSP27 stabilizes the actin CSK (21, 30, 47, 48). We reasoned that the decrease in bead motions reflects increases in CSK stability; if so, then ASM cells treated with arsenite, which causes HSP27 phosphorylation, would be expected to resist the effects of the actin-disrupting agent cytochalasin-D on bead motions. ASM cells treated for 1 h with 200 μM arsenite exhibited a decrease in bead motions and, more importantly, showed restricted bead motions even after a 10-min challenge with 1 μM cytochalasin-D (Fig. 7; *protocol 1*). This is in agreement with earlier findings by Guay and colleagues (21), who demonstrated, in Chinese hamster CCL39 cells, that treatment with arsenite before exposure to cytochalasin-D protects actin CSK structures. By contrast, ASM cells treated for 10 min with 1 μM cytochalasin-D, without prior treatment with arsenite, exhibited an increase in bead motions that remained elevated even after 1 h (Fig. 7; *protocol 3*). Interestingly, however, exposing the cytochalasin-D-treated ASM cells for the same duration (1 h) with arsenite (Fig. 7; *protocol 2*) caused a substantial decrease in bead motions and thereby reversed the effects of cytochalasin-D on bead motions. Although we have not explored the mechanisms that lead to those changes in bead motions, we speculate that the phosphorylated state of HSP27 may have a direct effect on F-actin formation and/or compete for the binding sites with cytochalasin-D, thereby providing structural stability to the CSK.

To directly assess the specific contribution of HSP27 to CSK stability, cultured rat ASM cells were transiently transfected to overexpress either HSP27-wt, HSP27-uP, or HSP27-P mutants. The human HSP27 and its mutant constructs have been

previously well characterized by others (3, 17, 28, 43, 63), and their expressions have been established in many cell types (26, 31, 36, 41, 47, 48, 52, 59). In this study, we verified the expression of human HSP27 proteins in cultured rat ASM cells by Western blotting, but we did not quantify the expression. ASM cells transfected with HSP27-wt or HSP27-uP both exhibited an increase in bead motions but, more interestingly, to a different extent: cells overexpressing HSP27-wt showed dramatic increases in bead motions, whereas cell overexpressing HSP27-uP showed slight increases in bead motions compared with either untransfected controls or GFP-transfected cells (Fig. 8*C*). By contrast, ASM cells transfected with HSP27-P showed a dramatic decrease in bead motions compared with the untransfected and the other transfected cells (Fig. 8*C*). Similarly, stably transfected cell lines of rat pulmonary microvascular endothelium overexpressing HSP27-P (36) also exhibited a substantial decrease in bead motions (unpublished data). These cell lines demonstrate reorganization of the actin CSK and the formation of stress fibers (36).

Under baseline conditions, the increases in bead motions for cells overexpressing HSP27-wt or HSP27-uP were substantially bigger than for cells overexpressing HSP27-P. This is consistent with the findings by others (5, 20, 26, 27, 47, 48, 55, 56, 59, 63) that HSP27 (unphosphorylated form) binds to actin microfilaments at the barbed ends and inhibits actin polymerization; this inhibition in turn is alleviated by the phosphorylation of HSP27. As regards the different extent of increase in bead motions, we postulate that the expressed human HSP27-wt is perhaps better able than the HSP27-uP to interact with endogenous HSP27 to form aggregates, to bind actin microfilaments, and/or to modulate the basal phosphorylation levels of HSP27 in cultured rat ASM cells, all of which may lead to decreases in actin polymerization, thereby resulting in the observed increases in bead motions.

In response to arsenite, cells overexpressing HSP27-wt or HSP27-uP both exhibited a decrease in bead motions, however. The extent to which arsenite caused a decrease in bead motions for cells overexpressing HSP27-uP (~35%) was similar to that of the controls (untransfected and GFP-transfected cells) but was less than that of the HSP27-wt (~44%); arsenite did not cause further decrease in bead motions for cells overexpressing HSP27-P. In fact, the measured bead motions of ASM cells overexpressing HSP27-P were comparable to the decrease in bead motions of other transfected cells after a 1-h treatment with 200 μM arsenite. Thus the extent of decrease in bead motions in response to arsenite was perhaps consistent with the supposed ability of these mutant proteins to be phosphorylated. These findings, taken together, support the notion that the expressed human HSP27-wt in cultured rat ASM cells is better able to interact with endogenous proteins as well as signals that lead to actin polymerization and, more importantly, suggest that the phosphorylated state of HSP27 is important for the stabilization of the actin CSK. Thus mechanical data obtained in the rat ASM cell are consistent with the reported structural changes (21, 36) and further confirm that HSP27 tethers bead motions only when phosphorylated.

Conclusion. The ability of the CSK to deform, to flow, and to reorganize its internal structures represents basic biological processes that underlie a variety of higher cell functions. In asthma, atherosclerosis, and angiogenesis, smooth muscle cells are exposed to growth factors and proinflammatory cytokines that contribute to CSK remodeling (64, 69, 74). In this study, we have shown that HSP27 phosphorylation is involved and likely plays a central part in those CSK remodeling processes. We have used spontaneous motions of beads anchored to the CSK as a quantitative index of the rate of ongoing microstructural rearrangements. These spontaneous motions were superdiffusive. Phosphorylation of HSP27 was found to tether bead motions, thereby providing the first direct functional evidence that activation of HSP27 indeed stabilizes the CSK and decreases the rate of microstructral reorganization.

ACKNOWLEDGMENTS

This study was supported by National Heart, Lung, and Blood Institute Grants HL-07118, HL-33009, HL-59682, and HL-48183.

REFERENCES

1. **An SS, Laudadio RE, Lai J, Rogers RA, and Fredberg JJ.** Stiffness changes in cultured airway smooth muscle cells. *Am J Physiol Cell Physiol* 283: C792–C801, 2002.
2. **Anderson CM, Georgious GN, Morrison IEG, Stevenson GVW, and Cherry RJ.** Tracking of cell surface receptors by fluorescence digital imaging microscopy using a charge-coupled device camera. *J Cell Sci* 101: 415–425, 1992.
3. **Arrigo AP and Welch WJ.** Characterization and purification of the small 28,000-dalton mammalian heat shock protein. *J Biol Chem* 262: 15359–15369, 1987.
4. **Balaban NQ, Schwartz US, Riveline D, Goichberg P, Tzur G, Sabanay I, Mahalu D, Safran S, Bershadsky A, Addadi L, and Geiger B.** Force and focal adhesion assembly: a close relationship studied using elastic micropatterned substrates. *Nat Cell Biol* 3: 466–472, 2001.
5. **Benndorf R, Haye K, Ryazantsev S, Wieske M, Behlke J, and Lutsch G.** Phosphorylation and supramolecular organization of murine small heat shock protein HSP25 abolish its actin polymerization-inhibiting activity. *J Biol Chem* 269: 20780–20784, 1994.
6. **Bitar KN, Kaminski MS, Hailat N, Cease KB, and Strahler JR.** HSP27 is a mediator of sustained smooth muscle contraction in response to bombesin. *Biochem Biophys Res Commun* 181: 1192–1200, 1991.
7. **Black JL and Johnson PR.** Airway smooth muscle in asthma. *Respirology* 1: 153–158, 1996.
8. **Carper SW, Rocheleau TA, and Storm FK.** cDNA sequence of a human heat shock protein HSP27. *Nucleic Acids Res* 18: 6457, 1990.
9. **Cooper JA.** Effects of cytochalasin and phalloidin on actin. *J Cell Biol* 105: 1473–1478, 1987.
10. **Coue M, Brenner SL, Spector I, and Korn ED.** Inhibition of actin polymerization by latrunculin A. *FEBS Lett* 213: 316–318, 1987.
11. **Edlund S, Landstrom M, Heldin CH, and Aspenstrom P.** Transforming growth factor-beta-induced mobilization of actin cytoskeleton requires signaling by small GTPases Cdc42 and RhoA. *Mol Biol Cell* 13: 902–914, 2002.
12. **Engel L and Ryan U.** TGF-beta 1 reverses PDGF-stimulated migration of human aortic smooth muscle cells in vitro. *In Vitro Cell Dev Biol Anim* 33: 443–451, 1997.
13. **Fabry B and Fredberg JJ.** Remodeling of the airway smooth muscle cell: are we built of glass? *Respir Physiol Neurobiol* 137: 109–124, 2003.
14. **Fabry B, Maksym GN, Shore SA, Moore PE, Panettieri RA Jr, Butler JP, and Fredberg JJ.** Time course and heterogeneity of contractile responses in cultured human airway smooth muscle cells. *J Appl Physiol* 91: 986–994, 2001.
15. **Feder J.** *Fractals.* New York: Plenum, 1988.
16. **Frohli E, Aoyama A, and Klemenz R.** Cloning of the mouse *hsp25* gene and an extremely conserved *hsp25* pseudogene. *Gene* 128: 273–277, 1993.
17. **Gaestel M, Schroder W, Benndorf R, Lippmann C, Buchner K, Hucho F, Erdmann VA, and Bielka H.** Identification of the phosphorylation sites of the murine small heat shock protein hsp25. *J Biol Chem* 266: 14721–14724, 1991.
18. **Gaestel M, Gross B, Benndorf R, Strauss M, Schunk WH, Kraft R, Otto A, Bohm H, Stahl J, Drabsch H, and Bielka H.** Molecular cloning, sequencing and expression in *Escherichia coli* of the 25-kDa growth-related protein of Ehrlich ascites tumor and its homology to mammalian stress proteins. *Eur J Biochem* 179: 209–213, 1989.

19. **Gaestel M, Gotthardt R, and Muller T.** Structure and organization of a murine gene encoding small heat-shock protein Hsp25. *Gene* 128: 279–283, 1993.
20. **Geum D, Son GH, and Kim K.** Phosphorylation-dependent cellular localization and thermoprotective role of heat shock protein 25 in hippocampal progenitor cells. *J Biol Chem* 277: 19913–19921, 2002.
21. **Guay J, Lambert H, Gingras-Breton G, Lavoie JN, Huot J, and Landry J.** Regulation of actin filament dynamics by p38 map kinase-mediated phosphorylation of heat shock protein 27. *J Cell Sci* 110: 357–368, 1997.
22. **Gunst SJ and Fredberg JJ.** The first three minutes: smooth muscle contraction, cytoskeletal events and soft glasses. *J Appl Physiol* 95: 413–425, 2003.
23. **Gunst SJ, Meiss RA, Wu MF, and Rowe M.** Mechanisms for the mechanical plasticity of tracheal smooth muscle. *Am J Physiol Cell Physiol* 268: C1267–C1276, 1995.
24. **Gunst SJ and Wu MF.** Plasticity of airway smooth muscle stiffness and extensibility: role of length-adaptive mechanisms. *J Appl Physiol* 90: 741–749, 2001.
25. **Halayko AJ, Camoretti-Mercado B, Forsythe SM, Vieira JE, Mitchell RW, Wylam ME, Hershenson MB, and Solway J.** Divergent differentiation paths in airway smooth muscle culture: induction of functionally contractile myocytes. *Am J Physiol Lung Cell Mol Physiol* 276: L197–L206, 1999.
26. **Hedges JC, Dechert MA, Yamboliev LA, Martin JL, Hickey E, Weber LA, and Gerthoffer WT.** A role for $p38^{MAPK}$/HSP27 pathway in smooth muscle cell migration. *J Biol Chem* 274: 24211–24219, 1999.
27. **Heldman AW, Kandzari DE, Tucker RW, Crawford LE, Fearon ER, Koblan KS, and Goldschmidt-Clermont PJ.** EJ-Ras inhibits phospholipase C gamma 1 but not actin polymerization induced by platelet-derived growth factor-BB via phosphatidylinositol 3-kinase. *Circ Res* 78: 312–321, 1996.
28. **Hickey E, Brandon SE, Potter R, Stein G, Stein J, and Weber LA.** Sequence and organization of genes encoding the human 27 kDa heat shock protein. *Nucleic Acids Res* 14: 4127–4145, 1986.
29. **Hubmayr RD, Shore SA, Fredberg JJ, Planus E, Panettieri RA, Moller W, Heyder J, and Wang N.** Pharmacological activation changes stiffness of cultured human airway smooth muscle cells. *Am J Physiol Cell Physiol* 271: C1660–C1668, 1996.
30. **Huot J, Houle F, Marceau F, and Landry J.** Oxidative stress-induced actin reorganization mediated by the p38 mitogen-activated protein kinase/heat shock protein 27 pathway in vascular endothelial cells. *Circ Res* 80: 383–392, 1997.
31. **Huot J, Lambert H, Lavoie JN, Guimond A, House F, and Landry J.** Characterization of 45-kDa/54-kDa HSP27 kinase, a stress-sensitive kinase which may activate the phosphorylation-dependent protective function of mammalian 27-kDa heat-shock protein HSP27. *Eur J Biochem* 227: 418–427, 1995.
32. **Ibitayo AI, Sladick J, Tuteja S, Louis-Jacques O, Yamada H, Groblewski G, Welsh M, and Bitar KN.** HSP27 in signal transduction and association with contractile proteins in smooth muscle cells. *Am J Physiol Gastrointest Liver Physiol* 277: G445–G454, 1999.
33. **Jakob U, Gaestel M, Engel K, and Buchner J.** Small heat shock proteins are molecular chaperones. *J Biol Chem* 268: 1517–1520, 1993.
34. **Kato K, Goto G, Inaguma Y, Hasegawa K, Morishita R, and Asano T.** Purification and characterization of a 20-kDa protein that is highly homologous to αβ crystalline. *J Biol Chem* 269: 15302–15309, 1994.
35. **Kato K, Ito H, Iwamoto I, Lida K, and Inaguma Y.** Protein kinase inhibitors can suppress stress-induced dissociation of Hsp27. *Cell Stress Chaperones* 6: 16–20, 2001.
36. **Kayyali US, Pennella CM, Trujillo C, Villa O, Gaestel M, and Hassoun PM.** Cytoskeletal changes in hypoxic pulmonary endothelial cells are dependent on MAPK-activated protein kinase MK2. *J Biol Chem* 277: 42596–42602, 2002.
37. **King GG, Pare PD, and Seow CY.** The mechanics of exaggerated airway narrowing in asthma: the role of smooth muscle. *Respir Physiol* 118: 1–13, 1999.
38. **Kubo R.** Brownian motion and nonequilibrium statistical mechanics. *Science* 233: 330–334, 1986.
39. **Kucik DF, Elson EL, and Sheetz MP.** Forward transport of glycoproteins on leading lamellipodia in locomoting cells. *Nature* 340: 315–317, 1989.
40. **Kuo KH, Wang L, Pare PD, Ford LE, and Seow CY.** Myosin thick filament lability induced by mechanical strain in airway smooth muscle. *J Appl Physiol* 90: 1811–1816, 2001.
41. **Landry J, Chretien P, Lambert H, Hickey E, and Weber LA.** Heat shock resistance conferred by expression of the human HSP27 gene in rodent cells. *J Cell Biol* 109: 7–15, 1989.
42. **Landry J and Huot J.** Modulation of actin dynamics during stress and physiological stimulation by a signaling pathway involving p38 MAP kinase and heat shock protein 27. *Biochem Cell Biol* 73: 703–707, 1995.
43. **Landry J, Lambert H, Zhou M, Lavoie JN, Hickey E, Weber LA, and Anderson CW.** Human HSP27 is phosphorylated at serine 78 and 82 by heat shock and mitogen-activated kinases that recognize the same amino acid motif as S6 kinase II. *J Biol Chem* 267: 794–803, 1992.
44. **Larsen JK, Yamboliev LA, Weber LA, and Gerthoffer WT.** Phosphorylation of the 27-kDa heat shock protein via p38 MAP kinase and MAPKAP kinase in smooth muscle. *Am J Physiol Lung Cell Mol Physiol* 273: L930–L940, 1997.
45. **Lauffenburger DA and Horwitz AF.** Cell migration: a physically integrated molecular process. *Cell* 84: 359–369, 1996.
46. **Lavoie J, Chretien P, and Landry J.** Sequence of the Chinese hamster small heat shock protein HSP27. *Nucleic Acids Res* 18: 1637, 1990.
47. **Lavoie JN, Gingras-Breton G, Tanguay RM, and Landry J.** Induction of Chinese hamster HSP27 gene expression in mouse cells confers resistance to heat shock. *J Biol Chem* 268: 3420–3429, 1993.
48. **Lavoie JN, Lambert H, Hickey E, Weber LA, and Landry J.** Modulation of cellular thermoresistance and actin filament stability accompanies phosphorylation-induced changes in the oligomeric structure of heat shock protein 27. *Mol Cell Biol* 15: 505–516, 1995.
49. **Ludwig S, Hoffmeyer A, Goebeler M, Kilian K, Hafners H, Neufeld B, Han J, and Rapp UR.** The stress inducer arsenite activates mitogen-activated protein kinases extracellular signal-regulated kinases 1 and 2 via a MAPK kinase 6/p38-dependent pathway. *J Biol Chem* 273: 1917–1922, 1998.
50. **Ma X, Wang Y, and Stephens NL.** Serum deprivation induces a unique hypercontractile phenotype of cultured smooth muscle cells. *Am J Physiol Cell Physiol* 274: C1206–C1214, 1998.
51. **Maksym GN, Fabry B, Butler JP, Navajas D, Tschumperlin DJ, Laporte JD, and Fredberg JJ.** Mechanical properties of cultured human airway smooth muscle cells from 0.05 to 0.4 Hz. *J Appl Physiol* 89: 1619–1632, 2000.
52. **Mehlen P, Preville X, Chareyron P, Briolay J, Klemenz R, and Arrigo AP.** Constitutive expression of human hsp27, Drosophila hsp27, or human αβ-crystallin confers resistance to TNF- and oxidative stress-induced cytotoxicity in stably transfected murine L929 fibroblasts. *J Immunol* 154: 363–374, 1995.
53. **Mehta D and Gunst SJ.** Actin polymerization stimulated by contractile activation regulates force development in canine tracheal smooth muscle. *J Physiol* 519: 829–840, 1999.
54. **Merck KB, Groenen PJ, Voorter CE, de Haard-Hoekman WA, Horwitz J, Bloemendal H, and de Jong WW.** Structural and functional similarities of bovine alpha-crystallin and mouse small heat-shock protein. A family of chaperone. *J Biol Chem* 268: 1046–1052, 1993.
55. **Miron T, Vancompernolle K, Vandekerckhove J, Wilchek M, and Geiger B.** A 25-kD inhibitor of actin polymerization is a low molecular mass heat shock protein. *J Cell Biol* 114: 255–261, 1991.
56. **Miron T, Wilcheck M, and Geiger B.** Characterization of an inhibitor of actin polymerization in vinculin-rich fraction of turkey gizzard smooth muscle. *Eur J Biochem* 178: 543–553, 1988.
57. **Pantaloni D, Le Clainche C, and Carlier MF.** Mechanisms of actin-based motility. *Science* 292: 1502–1506, 2001.
58. **Parker KK, Brock AL, Brangwynne C, Mannix RJ, Wang N, Ostuni E, Geisse NA, Adams JC, Whitesides GM, and Ingber DE.** Directional control of lamellipodia extension by constraining cell shape and orienting cell tractional forces. *FASEB J* 16: 1195–1204, 2002.
59. **Piotrowicz RS and Levin EG.** Basolateral membrane-associated 27-kDa heat shock protein and microfilament polymerization. *J Biol Chem* 272: 25920–25927, 1997.
60. **Porter AC, Fanger GR, and Vaillancourt RR.** Signal transduction pathways regulated by arsenate and arsenite. *Oncogene* 18: 7794–7802, 1999.
61. **Pratusevich VR, Seow CY, and Ford LE.** Plasticity in canine airway smooth muscle. *J Gen Physiol* 105: 73–94, 1995.
62. **Probstein RF.** *Physicochemical Hydrodynamics.* Stoneham, MA: Butterworths, 1989.

63. **Rogalla T, Ehrnsperger M, Preville X, Kotlyarov A, Lutsch G, Ducasse C, Paul C, Wieske M, Arrigo AP, Buchner J, and Gaestel M.** Regulation of Hsp27 oligomerization, chaperone function, and protective activity against oxidative stress/tumor necrosis factor α by phosphorylation. *J Biol Chem* 274: 18947–18956, 1999.
64. **Ross R.** The pathogenesis of atherosclerosis: a perspective for the 1990s. *Nature* 362: 801–809, 1993.
65. **Rouse J, Cohen P, Trigon S, Morange M, Alonso-Lamazares A, Zamanillo D, Hunt T, and Nebreda AR.** A novel kinase cascade triggered by stress and heat shock that stimulates MAPKAP kinase-2 and phosphorylation of the small heat shock proteins. *Cell* 78: 1027–1037, 1994.
66. **Saxton MJ and Jacobson K.** Single-particle tracking: applications to membrane dynamics. *Annu Rev Biophys Biomol Struct* 26: 373–399, 1997.
67. **Schmidt CE, Chen T, and Lauffenburger DA.** Simulation of integrin-cytoskeletal interactions in migrating fibroblasts. *Biophys J* 67: 461–474, 1994.
68. **Schmidt CE, Horwitz AF, Lauffenburger DA, and Sheetz MP.** Integrin-cytoskeletal interactions in migrating fibroblasts are dynamic, asymmetric, and regulated. *J Cell Biol* 123: 977–991, 1993.
69. **Schwartz SM.** Smooth muscle migration in atherosclerosis and restenosis. *J Clin Invest* 100: S87–S89, 1997.
70. **Seow CY and Fredberg JJ.** Historical perspective on airway smooth muscle: the saga of a frustrated cell. *J Appl Physiol* 91: 938–952, 2001.
71. **Seow CY, Pratusevich VR, and Ford LE.** Series-to-parallel transition in the filament lattice of airway smooth muscle. *J Appl Physiol* 89: 869–876, 2000.
72. **Spiro TP and Mundy GR.** In vitro migration of Walker 256 carcinosarcoma cells: dependence on microtubule and microfilament function. *J Natl Cancer Inst* 65: 463–467, 1980.
73. **Stamenovic D, Mijailovich SM, Tolic-Norrelykke IM, Chen J, and Wang N.** Cell prestress. II. Contribution of microtubules. *Am J Physiol Cell Physiol* 282: C617–C624, 2002.
74. **Stewart AG, Tomlinson PR, and Wilson J.** Airway wall remodeling in asthma: a novel target for the development of anti-asthma drugs. *Trends Pharmacol Sci* 14: 275–279, 1993.
75. **Sun HQ, Yamamoto M, Mejillano M, and Yin HL.** Gelsolin, a multifunctional actin regulatory protein. *J Biol Chem* 274: 33179–33182, 1999.
76. **Wang N.** Mechanical interactions among cytoskeletal filaments. *Hypertension* 32: 162–165, 1998.
77. **Wang N, Butler JP, and Ingber DE.** Mechanotransduction across the cell surface and through the cytoskeleton. *Science* 260: 1124–1127, 1993.
78. **Wang L, Pare PD, and Seow CY.** Effects of length oscillation on the subsequent force development in swine tracheal smooth muscle. *J Appl Physiol* 88: 2246–2250, 2000.
79. **Wang L, Pare PD, and Seow CY.** Effects of chronic passive length change on smooth muscle length-tension relationship. *J Appl Physiol* 90: 734–740, 2001.
80. **Wong JZ, Woodcock-Mitchell J, Mitchell J, Rippetoe P, White S, Absher M, Baldor L, Evans J, McHugh KM, and Low RB.** Smooth muscle actin and myosin expression in cultured airway smooth muscle cells. *Am J Physiol Lung Cell Mol Physiol* 274: L786–L792, 1998.
81. **Woolcock AJ and Peat JK.** Epidemiology of bronchial hyperresponsiveness. *Clin Rev Allergy Immunol* 7: 245–256, 1989.